Oxidative Decomposition of Propylene Carbonate in Lithium Ion Batteries: A DFT Study

ARTICLE *in* THE JOURNAL OF PHYSICAL CHEMISTRY A · JULY 2013

Impact Factor: 2.69 · DOI: 10.1021/jp403436u · Source: PubMed

5 AUTHORS, INCLUDING:

Ermias Girma Leggesse
National Taiwan University of Science and Tec…
19 PUBLICATIONS **38** CITATIONS
SEE PROFILE

Jyh-Chiang Jiang
National Taiwan University of Science and Tec…
174 PUBLICATIONS **2,612** CITATIONS
SEE PROFILE

THE JOURNAL OF PHYSICAL CHEMISTRY A

Article

pubs.acs.org/JPCA

Oxidative Decomposition of Propylene Carbonate in Lithium Ion Batteries: A DFT Study

Ermias Girma Leggesse, Rao Tung Lin, Tsung-Fan Teng, Chi-Liang Chen, and Jyh-Chiang Jiang*

Department of Chemical Engineering, National Taiwan University of Science and Technology, Taipei 106, Taiwan, R.O.C.

Supporting Information

ABSTRACT: This paper reports an in-depth mechanistic study on the oxidative decomposition of propylene carbonate in the presence of lithium salts ($LiClO_4$, $LiBF_4$, $LiPF_6$, and $LiAsF_6$) with the aid of density functional theory calculations at the B3LYP/6-311++G(d,p) level of theory. The solvent effect is accounted for by using the implicit solvation model with density method. Moreover, the rate constants for the decompositions of propylene carbonate have been investigated by using transition-state theory. The shortening of the original carbonyl C−O bond and a lengthening of the adjacent ethereal C−O bonds of propylene carbonate, which occurs as a result of oxidation, leads to the formation of acetone radical and CO_2 as a primary oxidative decomposition product. The termination of the primary radical generates polycarbonate, acetone, diketone, 2-(ethan-1-ylium-1-yl)-4-methyl-1,3-dioxolan-4-ylium, and CO_2. The thermodynamic and kinetic data show that the major oxidative decomposition products of propylene carbonate are independent of the type of lithium salt. However, the decomposition rate constants of propylene carbonate are highly affected by the lithium salt type. On the basis of the rate constant calculations using transition-state theory, the order of gas volume generation is: $[PC\text{-}ClO_4]^-$ > $[PC\text{-}BF_4]^-$ > $[PC\text{-}AsF_6]^-$ > $[PC\text{-}PF_6]^-$.

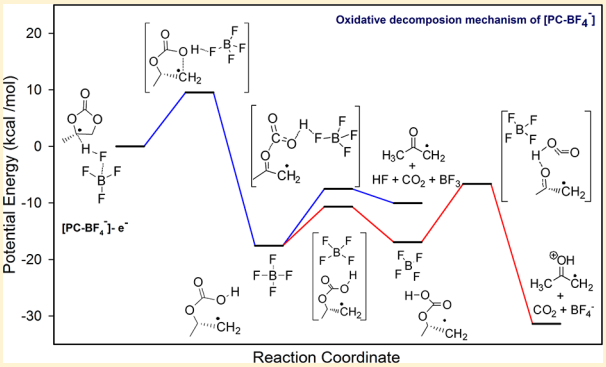

INTRODUCTION

Lithium-ion batteries are used in various portable electric devices such as cell phones and laptops because they offer several advantages over other types of rechargeable batteries, including high energy density, lightweight design, and longer lifespan.[1−4] They are also a promising source of energy for hybrid electric vehicles (HEVs) and plug-in hybrid electric vehicles (PHEVs), along with other applications.[5] Owing to the current game-changing increase in demand for lithium-ion batteries, starting from cell phones and web-enabled tablet devices to HEVs, they are being considered as a leading contender for a clean and sustainable energy source.

A typical lithium ion battery system is made up of transition-metal oxide such as $LiMn_2O_4$, $LiCoO_2$, and $LiNiO_2$ as cathode, a carbonaceous electrode as an anode, and electrolyte solution, which is commonly a lithium salt dissolved in a mixture of organic solvents. Among the components of lithium ion battery, the type and electrochemical properties of cathode materials are determining factors regarding cost, weight, and efficiency of the battery. During the past few years, a lot of progress has been made in identifying new, improved high-capacity cathode materials that can overcome most of the challenges that the current lithium ion battery technology faces.[6−8] However, the electrochemical potential of most of these proposed materials is far beyond the thermodynamic stability window of commonly used organic electrolytes. It has been reported that[9] at both open-circuit and during cell charge the high potentials of various cathode materials may result in electrolyte oxidation. The highly exothermic electrolyte decomposition reactions are usually accompanied by the decomposition of the cathode material and gas evolution, which will increase the internal pressure of the electrochemical cell.[10] The increase in the internal pressure will certainly cause potential danger and reduced cyclic stability.[11−13]

Today's lithium ion batteries contain cyclic and acyclic diesters of carbonic acids as electrolyte solvents because these compounds are relatively stable for electrochemical oxidation compared with ethers.[14] Among these solvents, propylene carbonate (PC), diethyl carbonate (DEC), ethylene carbonate (EC), and dimethyl carbonate (DMC) have attracted much research attention owing to their physicochemical properties. EC and PC are well-known solvents with relatively high oxidation potentials, which are around 5.0 V. However, compared with EC, PC is the most labile toward oxidation.[15] Hence, to utilize these solvents for high-voltage lithium ion batteries, oxidation of the solvents must be understood because their oxidation potentials are close to the maximum charge voltage of the current lithium ion battery cells.

Even though the detection of the protective film on the cathode surface has not been as straightforward as the solid

Received: April 8, 2013
Revised: July 10, 2013
Published: July 22, 2013

   dx.doi.org/10.1021/jp403436u | J. Phys. Chem. A 2013, 117, 7959−7969

electrolyte interface formed on the anode, it is believed that oxidative decomposition products of electrolytes are the major components of the film formed on the cathode surface.[14,16] Aurbach et al.[17] examined the interfacial behavior of different cathode materials using electrochemical impedance spectroscopy and found that the surface film formation on the cathode surface increases the electrode impedance and even electrically isolates part of the active mass. The influence of the surface film formation on the performance of the cathode materials will become noticeable at elevated temperatures, resulting from pronounced surface-related capacity fading due to the development of higher electrode impedance. Kanamura et al.[18,19] showed that the electrochemical oxidation processes of organic solvents, such as PC, are influenced by the type of electrolyte salt used. Similarly, Arakawa et al.[20] used GC/MS to investigate the oxidative decomposition products of PC containing different lithium salts and reported the formation of CO_2, CO, alkanes, and *cis*- and *trans*-2-ethyl-4-methyl-1,3-dioxolane on the surface of the cathode.

The understanding of the protective film formed on the cathode surface is essential for the quest to produce lithium ion batteries that can deliver higher levels of energy while maintaining safety. However, there have been relatively fewer studies dedicated to the understanding of this very issue.[21−23] As a result, the formation mechanism and morphology of the protective layer formed on the positive electrodes is still one of the unsettled topics in lithium ion battery technology.

In this contribution, density functional theory (DFT) calculations have been carried out to propose detailed mechanisms for the oxidative decomposition reaction of PC in the presence of $LiPF_6$, $LiClO_4$, $LiBF_4$, and $LiAsF_6$. Moreover, the rate of gas generation during oxidative decomposition of the solvent is predicted by using transition-state theory.

COMPUTATIONAL DETAILS

As a result of relatively low computational demands, DFT methods are often used for studying reactions involving radicals,[21,23−26] such as similar systems discussed in this paper. However, regardless of their widespread use, studies have shown that DFT with the currently available approximate exchange-correlation functionals is subject to significant error.[27,28] Because the objective of this work is not to produce a highly accurate potential energy surface for the reactions studied, the method employed should be strong enough to provide the right trend for the barrier heights for a series of reactions. Previous studies also show that for reactions involving radicals hybrid DFT methods (such as B3LYP and BH&HLYP) that include exact HF exchange are better than pure DFT functionals and are close to the results generated from high-level ab initio theory calculations, such as CCSD-(T)/6-311++G(d,p) method.[29−31]

All of the theoretical investigation has been carried out employing DFT with the B3LYP method[32−35] using 6-311++G(d,p) basis set, as presented in the Gaussian 09 package.[36] Spin−unrestricted scheme was used for the odd numbers of electron systems to allow for any possible bond cleavage during geometry optimization. To confirm the transition states and make zero point energy (ZPE) corrections, frequency analyses were done with the same basis set as that for the geometry optimizations. Intrinsic reaction coordinate (IRC) calculations were also performed to verify whether the reaction pathway of individual chemical reaction correctly connects the stationary points under consideration. Unless otherwise stated, the relative energies represent those with ZPE correction, and Gibbs free energies and enthalpies are calculated at 298.15 K. The spin contamination was considered by comparison of the expectation value of the $<S^2>$ operator. $<S^2>$ before annihilation was generally between 0.75 and 0.77 for the doublet states, which is close to the doublet state S^2 value of 0.75;[37] confirming that the spin contamination would have an insignificant effect on the result. Natural bond orbital (NBO)[38] analysis was performed using the same level of theory.

The implicit solvent effect was accounted for by using the solvation model with density (SMD) method[39] as implemented in Gaussian 09, where the dielectric constant of 41.32 was chosen by considering EC/PC/DEC (3:2:5) solvent system in relation to the conditions implemented in the experiments.[40,41] The SMD model is based on integral-equation-formalism polarizable continuum model (IEF-PCM) protocol for bulk electrostatics that involve integration of the nonhomogeneous Poisson equation and on a cavity dispersion-solvent-structure protocol for the nonelectrostatic contribution to the free energy of solvation.[39]

To determine whether the rate of gas generation depends on the type of salt used, we employed transition-state theory[42] to determine the rate constants for the rate-determining steps. Assuming that all molecules that cross the barrier proceed to become products, the rate constant k at 298.15 K was calculated by using the following equation:

$$k(T) = \frac{k_B T}{h} \cdot \frac{Q(T)^{\neq}}{Q(T)} e^{-E^{\neq}/k_B T} \quad (1)$$

where k_B is the Boltzmann constant, $Q(T)$ and $Q(T)^{\neq}$ are partition functions for the reactant and transition state, respectively, and $E^{\neq}$ is the zero-point barrier for the reaction. Rotational, translational, vibrational, and electronic contributions to the partition functions are obtained after geometry optimizations.

RESULTS AND DISCUSSION

Thermodynamic Oxidation Potentials of PC−Anion Complexes. The optimized structures with selected structural parameters of PC-PF_6^-, PC-BF_4^-, PC-AsF_6^-, and PC-ClO_4^- calculated with SMD-B3LYP/6-311++G(d,p) in implicit solvent are shown in Figure S1 of the Supporting Information. To determine the electrochemical oxidation potentials of PC−anion complexes, thermodynamic cycles[43] as shown in Figure 1 are used to calculate the Gibbs free-energy change for Li/Li^+ and for the oxidation reaction of PC−anion complexes, respectively.

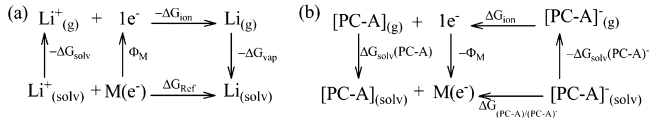

Figure 1. Thermodynamic cycles for lithium electrode reaction (a) and oxidation reactions of PC-anion complexes (b).

On the basis of the thermodynamic cycle for Li/Li^+, the free energy can be calculated by using eq 2:

$$\Delta G_{ref} = -\Delta G_{solv}(Li^+) + \phi_M - \Delta G_{vap}(Li) - \Delta G_{ion}(Li) \quad (2)$$

dx.doi.org/10.1021/jp403436u | J. Phys. Chem. A 2013, 117, 7959−7969

where $\Delta G_{solv}(Li^+)$ is the free energy of solvation of lithium cation in the solvent system under consideration, Φ_M is the work function of the electrode, $\Delta G_{vap}(Li)$ is the free energy of vaporization of lithium, and $\Delta G_{ion}(Li)$ is the calculated free energy of ionization of lithium. Similarly, the free energy for the solvent−anion complex ([PC-A]) oxidation reaction can be calculated using eq 3:

$$\Delta G_{[PC\text{-}A]/[PC\text{-}A^+]} = \Delta G_{solv}[PC\text{-}A^+] + \phi_M - \Delta G_{solv}[PC\text{-}A] - \Delta G_{ion}[PC\text{-}A] \quad (3)$$

The thermodynamic oxidation potentials for PC−anion complexes versus Li/Li^+ can be derived by taking the deference between eqs 2 and 3, as shown in eq 4. The free energy of vaporizations for lithium and the solvent are standards,[44] while the solvation free energies and free energies of ionization are calculated with SMD-B3LYP/6-311++G(d,p).

$$E_{OX}[Li/Li^+] = \frac{-(\Delta G_{[PC\text{-}A]/[PC\text{-}A^+]} + \Delta G_{ref})}{F} = -\frac{1}{F}(\Delta G_{solv}[PC\text{-}A^+] - \Delta G_{solv}[PC\text{-}A] - \Delta G_{ion}[PC\text{-}A] - \Delta G_{solv}(Li^+) - \Delta G_{vap}(Li) - \Delta G_{ion}(Li)) \quad (4)$$

The calculated oxidation potentials of PC−anion complexes are listed in Table 1. It can be seen that the values for the calculated oxidation potentials are in better agreement with the experimentally reported data[14,45−47] than previously reported findings by Xing et al.[22] The small variation from the experimentally reported results exists because the experimental oxidation potentials are not the real thermodynamics potential but are found by approximation based on kinetic measurements.

Table 1. Calculated Electrochemical Oxidation Potentials (V) for PC−Anion Complexes with Experimental Values and Previous Reported Data Shown for Comparison

structure	E_{ox} (calculated)	E_{ox} (experimental)[a]	previous reports[b]
$[PC\text{-}PF_6]^-$	6.67	6.80	6.47
$[PC\text{-}BF_4]^-$	6.22	6.60	
$[PC\text{-}AsF_6]^-$	6.76	6.80	
$[PC\text{-}ClO_4]^-$	5.34	5.20−5.60	5.57

[a]From refs 14 and 18. [b]From ref 22.

Oxidative Decomposition Mechanism for PC-PF_6^-, PC-BF_4^-, PC-AsF_6^-, and PC-ClO_4^-. Recent molecular dynamics simulations using Atomistic Polarizable Potential for Liquids, Electrolytes, & Polymers (APPLE&P) force field for prediction of thermodynamic and transport properties, showed that most of the lithium salt anions are not coordinated with lithium cations on the surface of the cathode.[48,49] Ions found in the "outer Helmholtz plane" are about two solvent-molecule diameters away from the electrode surface because both the ions and the electrode surface are solvated. Ions in the "inner Helmholtz plan", which are usually the weekly solvated, large anions such as PF_6^-, ASF_6^-, ClO_4^-, and BF_4^-, have the tendency to shed their solvation layer and penetrate the solvent layer on the electrode and form direct contact with the electrode surface. Hence, in our calculation we only consider solvent−anion complexes to propose plausible mechanisms for the oxidative decomposition reactions that can occur on the surface of the cathode material in lithium ion batteries.

To elucidate the most likely mechanism of bond breaking in the oxidized PC−anion complexes, we calculated bond orders of [PC-PF_6^-]-e, [PC-AsF_6^-]-e, [PC-BF_4^-]-e, and [PC-ClO_4^-]-e using the natural population analysis with natural localized molecular orbitals (NLMO/NPA). The bond orders in Table S1 in the Supporting Information confirm our assumption that the bond between the ethereal oxygen and alkyl carbon (O7−C1) is the weakest in all PC−anion complexes. The result indicates that after an electron is removed from PC−anion complexes, O7−C1 bond is weakened, which results in the breaking of the bond to form an open-chain cation radical. The potential-energy profile for the oxidative decomposition of PC-PF_6^- in solution is shown in Figure 2, and relative energies and Gibbs free energies are presented in Table 2. The Lewis acid−base adducts formed as a result of interaction of PC with the noncoordinating anion, PF_6^-, result in hyperconjugation between the acidic hydrogen adjacent to the methyl group. Upon removal of an electron from this adduct, the anion abstracts the acidic hydrogen, resulting in a radical species, as shown in Scheme 1, where the unpaired electron is located on the carbon atom from which the hydrogen is abstracted. The heterolytic ring-opening reaction could happen to [PC-PF_6^-]-e, which proceeds through a transition state, **TS1-1**, with a ring-opening barrier of 12.51 kcal mol^{-1} to give **M1-1**, which is yet another Lewis acid−base adduct that is a tertiary carbocation having unpaired electron on the terminal methylene group with a coefficient of 0.70, as confirmed by the spin density difference from NBO calculation. This radical carbocation could undergo decarboxylation reaction through a transition state, **TS1-4**, with an energy barrier of 13.80 kcal mol^{-1} to generate acetone radical, HF, CO_2, and PF_5.

An alternative to this path results in the formation of a relatively stable intermediate, **M1-2**, owing to a conformational change along the H−O−C−O dihedral angle passing through a transition state, **TS1-2**, which has a lower energy barrier than the aforementioned path. The enol form of acetone cation, CO_2, and PF_6^- are generated from **M1-2** through decarboxylation, which is identified as a rate-determining step in the oxidative decomposition reaction of PC-PF_6^-.

As can be seen in Schemes 1 and 2, from the reaction mechanism points of view, the oxidative decomposition mechanisms of PC-BF_4^- and PC-AsF_6^- follow a similar path as PC-PF_6^-. The potential-energy profiles for oxidative decomposition of PC-BF_4^- and PC-AsF_6^- in implicit solvent are shown in Figures 3 and 4, respectively. Furthermore, the relative energies and Gibbs free energies for the oxidative decomposition of PC-BF_4^- and PC-AsF_6^- are presented in Tables 3 and 4, respectively. Compared with the decomposition path of PC-PF_6^-, there is a significant difference in the energy barrier for the heterolytic ring-opening steps in the decomposition paths of PC-BF_4^- and PC-AsF_6^-. This change in ring-opening energy barrier (9.54 and 13.83 kcal mol^{-1} for PC-BF_4^- and PC-AsF_6^-, respectively) arises due to the difference in reactivity among PF_6^-, BF_4^-, and AsF_6^-. Unlike the five- and six-coordinated compounds of arsenic and phosphorus, BF_4^- is characterized by extensive charge delocalization owing to its symmetrical structure. Hence, rather than BF_3, which is formed at the initial oxidation step, the formation of BF_4^- as a result of intramolecular electron transfer

dx.doi.org/10.1021/jp403436u | J. Phys. Chem. A 2013, 117, 7959−7969

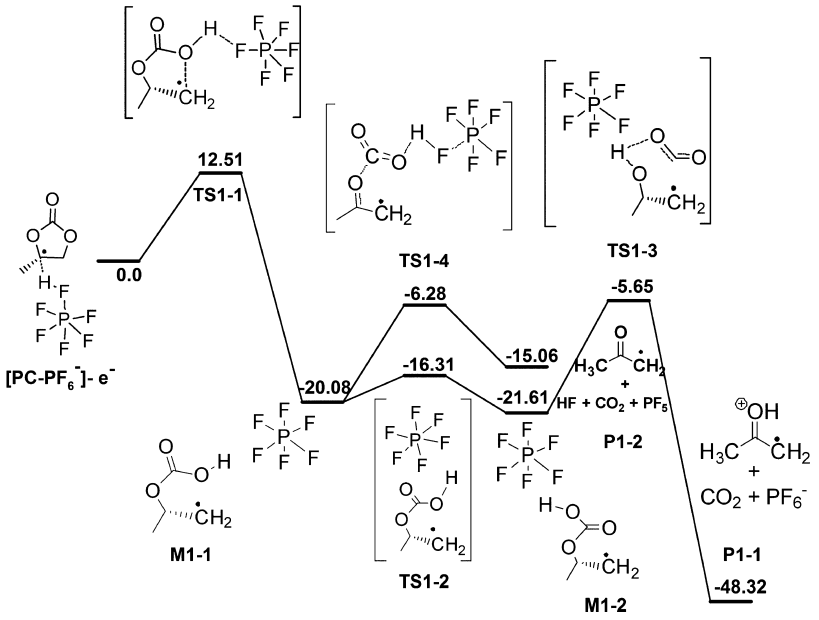

Figure 2. Potential-energy profile (kcal mol^{-1}) at 298.15 K for the oxidative decomposition mechanism of PC-PF_6^- calculated with SMD-B3LYP/6-311++G(d,p).

Table 2. Relative Energies, Enthalpies, Free Energies (in kcal mol^{-1}) of the Stationary Points, and Imaginary Frequencies (ω/cm^{-1}) of Transition States for Oxidative Decomposition of PC-PF_6^- Calculated with SMD-B3LYP/6-311++G(d,p)

structure	ΔE	ΔH	ΔG	ω
[PC-PF_6^-]-e	0	0	0	
TS1-1	12.51	8.16	8.79	−459
M1-1	−20.08	−19.48	−22.59	
TS1-2	−16.31	−19.45	−14.43	−288
M1-2	−21.61	−25.10	−26.98	
TS1-3	−5.65	−5.02	−5.64	−205
P1-1	−48.32	−47.06	−52.71	
TS1-4	−6.28	−6.27	−8.83	−399
P1-2	−15.06	−13.18	−20.71	

will be relatively easy, which is catalyzed by the acid formed in the initial step.

It should be noted that extensive charge delocalization in such anions, caused by strong electron-withdrawing substituents, will make the corresponding lithium salts produce sufficiently high ionic conductivity solutions with wide electrochemical stability windows and high thermal stability.[50,51] The energy barrier for the decarboxylation reaction, which resulted in the formation of acetone radical, is higher in PC-AsF_6^- than in PC-PF_6^- (18.82 vs 13.80 kcal mol^{-1}) owing to the relative chemical stability of AsF_6^-. On the base of the Lewis acid strength of the conjugate XF_5 (X = As or P) species, it can be explained that AsF_6^- is relatively a more chemically stable anion than PF_6^- because it has a stronger conjugate Lewis acid that will more effectively bind with the fluoride ion and form a more chemically stable anion.

Scheme 1. Oxidative Decomposition Mechanism of PC-XF_6^-, where X = P, As

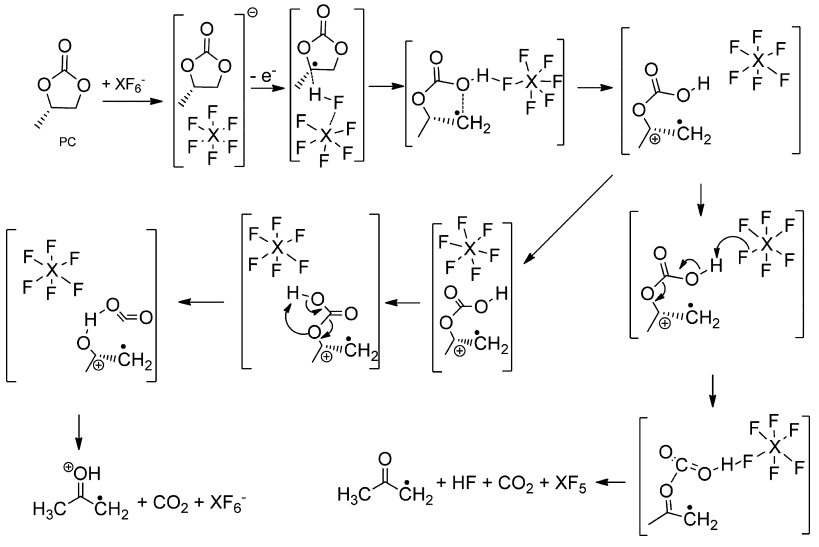

dx.doi.org/10.1021/jp403436u | J. Phys. Chem. A 2013, 117, 7959−7969

Scheme 2. Oxidative Decomposition Mechanism of PC-BF_4^-

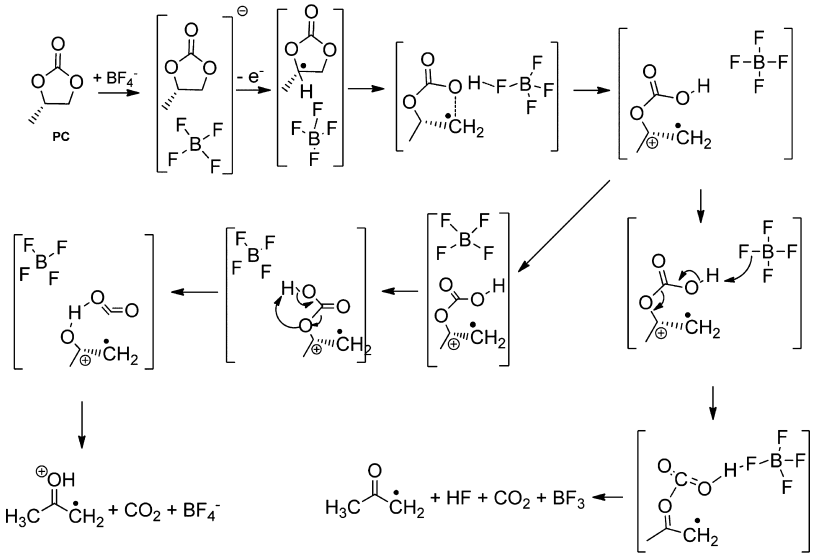

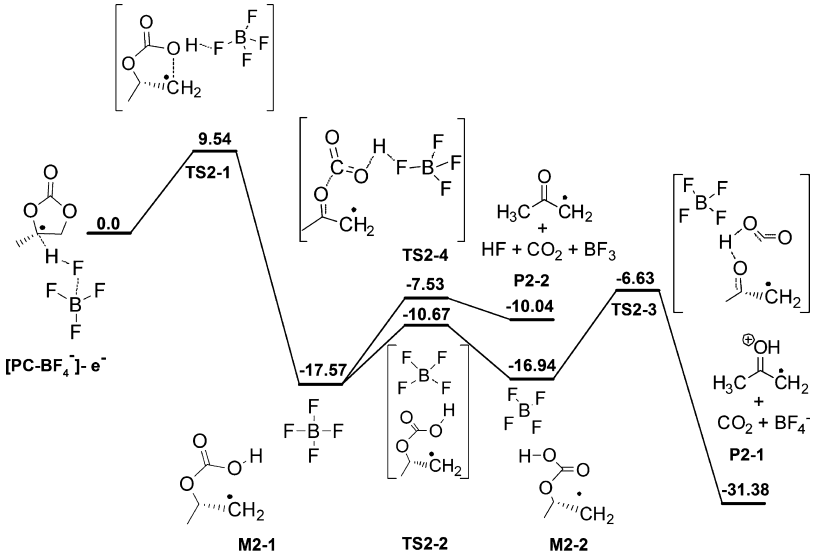

Figure 3. Potential energy profile (kcal mol^{-1}) at 298.15 K for the oxidative decomposition mechanism of PC-BF_4^- calculated with SMD-B3LYP/6-311++G(d,p).

As can be seen from Scheme 3, the oxidative decomposition mechanism of PC-ClO_4^- is significantly different from the fluorinated solvent−anion complexes that are discussed above. The potential-energy profile for the oxidative decomposition of PC-ClO_4^- in implicit solvent is shown in Figure 5, and relative energies and Gibbs free energies are presented in Table 5. Unlike the similar steps in the decomposition mechanisms of PC-PF_6^-, PC-BF_4^-, and PC-AsF_6^-, PC-ClO_4^-directly generates CO_2, $HClO_4$, and acetone radical as primary oxidation products. Moreover, owing to the fact that ClO_4^- is far less coordinating than BF_4^-, PF_6^-, and PF_6^-, the heterolytic ring-opening reaction could happen with a ring-opening barrier of 4.39 kcal mol^{-1} to give the expected compounds.

Table 6 depicts the change in enthalpies, Gibbs free energies, activation energy, and rate constants at 298.15 K for the rate-determining step in the oxidative decomposition of PC-PF_6^-, PC-AsF_6^-, and PC-BF_4^- and for the single oxidative decomposition steps of PC-ClO_4^-. The vibrational, electronic, translational, rotational, and molecular partition functions used in the calculation of the rate constants are shown in Table S2 in the Supporting Information. On the basis of the rate constants calculated using transition-state theory, the CO_2 generation in the presence of ClO_4 is higher than that in BF_4^-, followed by AsF_6^- and PF_6^-. Our calculated result is in agreement with the experimental observation by Arakawa et al., in which an intense gas evolution was reported as a result of PC oxidation containing $LiCO_4$ compared with the system containing $LiPF_6$.[20] Hence we can conclude that the order of gas volume generation is: [PC-ClO_4]$^-$ > [PC-BF_4]$^-$ > [PC-AsF_6]$^-$ > [PC-PF_6]$^-$.

Possible Termination Pathways for the Radical Cations. The termination reactions of the enol form of acetone cation radical, which is formed as a primary product in the oxidative decomposition reactions of PC-PF_6^-, PC-BF_4^-, and PC-AsF_6^-, are investigated comprehensively as presented in Scheme 4. The enol form of acetone cation radical, which is simply denoted **RC-1** hereafter, could undergo isomerization from the stable enol form to the keto isomer. Woodward et

dx.doi.org/10.1021/jp403436u | J. Phys. Chem. A 2013, 117, 7959−7969

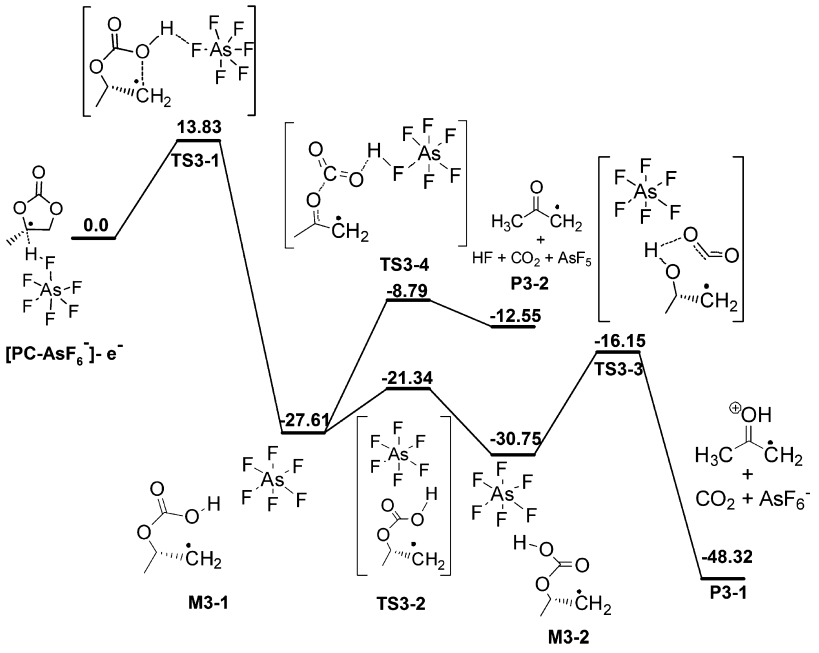

Figure 4. Potential-energy profile (kcal mol^{-1}) at 298.15 K for the oxidative decomposition mechanism of PC-AsF_6^- calculated with SMD-B3LYP/6-311++G(d,p).

Table 3. Relative Energies, Enthalpies, Free Energies (in kcal mol^{-1}) of the Stationary Points, and Imaginary Frequencies (ω/cm^{-1}) of Transition States for Oxidative Decomposition of PC-BF_4^- Calculated with SMD-B3LYP/6-311++G(d,p)

structure	ΔE	ΔH	ΔG	ω
[PC-BF_4^-]-e	0	0	0	
TS2-1	9.54	9.29	10.59	−474
M2-1	−17.57	17.70	−16.75	
TS2-2	−10.67	−13.93	−15.02	−398
M2-2	−16.94	−17.07	−15.5	
TS2-3	−6.63	−6.77	−7.09	−322
P2-1	−31.38	−30.87	−32.44	
TS2-4	−7.53	−6.91	−7.74	−348
P2-2	−10.67	−8.86	−12.46	

Table 4. Relative Energies, Enthalpies, Free Energies (in kcal mol^{-1}) of the Stationary Points, and Imaginary Frequencies (ω/cm^{-1}) of Transition States for Oxidative Decomposition of PC-AsF_6^- Calculated with SMD-B3LYP/6-311++G(d,p)

structure	ΔE	ΔH	ΔG	ω
[PC-AsF_6^-]-e	0	0	0	
TS3-1	13.83	13.82	13.83	−472
M3-1	−27.61	−25.00	−31.38	
TS3-2	−21.34	−18.82	−21.10	−326
M3-2	−30.75	−28.86	−32.63	
TS3-3	−16.15	−16.90	−19.66	−499
P3-1	−48.32	−48.94	−48.95	
TS3-4	−8.79	−6.01	7.10	−288
P3-2	−12.55	−13.00	−13.14	

al.,[52] concluded that superfacial 1,3-H-shift across double bonds will not occur because such reactions are symmetry-forbidden because it involves the overlap of orbitals with opposite signs. However, the symmetry-allowed antarafacial shift can occur but would require a strained transition state, containing a small twisted ring. On the basis of our calculation, the antarafacial 1,3

Scheme 3. Oxidative Decomposition Mechanism of PC-ClO_4^-

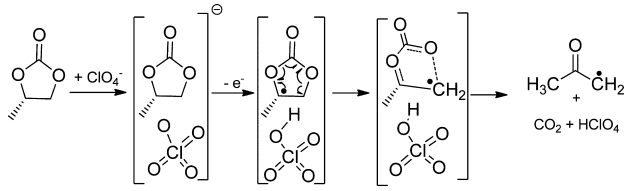

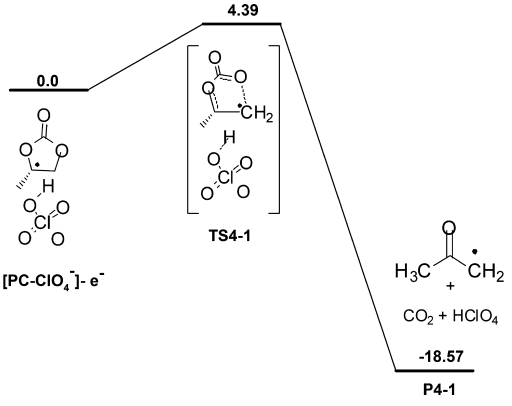

Figure 5. Potential-energy profile (kcal mol^{-1}) at 298.15 K for the oxidative decomposition mechanism of PC-ClO_4^- calculated with SMD-B3LYP/6-311++G(d,p).

Table 5. Relative Energies, Enthalpies, Free Energies (in kcal mol^{-1}) of the Stationary Points, and Imaginary Frequencies (ω/cm^{-1}) of Transition States for Oxidative Decomposition of PC-ClO_4^- Calculated with SMD-B3LYP/6-311++G(d,p)

structure	ΔE	ΔH	ΔG	ω
[PC-ClO_4^-]-e	0	0	0	
TS4-1	4.39	3.76	3.14	−415
P4-1	−18.57	−19.83	−20.08	

dx.doi.org/10.1021/jp403436u | J. Phys. Chem. A 2013, 117, 7959−7969

Table 6. Changes in Entropy and Gibbs Free Energy (in kcal mol^{-1}), Activation Energy (in kcal mol^{-1}), and Rate Constants at 298.15 K (in 1 mol^{-1} s^{-1}) Calculated for the Rate-Determining Steps in the Oxidative Decomposition Reactions of Solvent-Anion Complexes

			activation energy		
reaction	ΔH	ΔG	forward	backward	rate constant
M1-2 → TS1-3 → P1-1	−21.96	−25.73	15.96	42.67	1.7×10^{-9}
M2-2 → TS2-3 → P2-1	−13.80	−17.42	10.31	24.25	7.4×10^{-2}
M3-2 → TS3-3 → P3-1	−20.08	−16.32	14.60	32.17	5.7×10^{-8}
[PC-ClO_4^-]-e$^-$ → TS4-1 → P4-1	−19.83	−20.08	4.39	22.96	2.1×10^{3}

Scheme 4. Termination Path for RC-1 Calculated with SMD-B3LYP/6-311++G(d,p)[a]

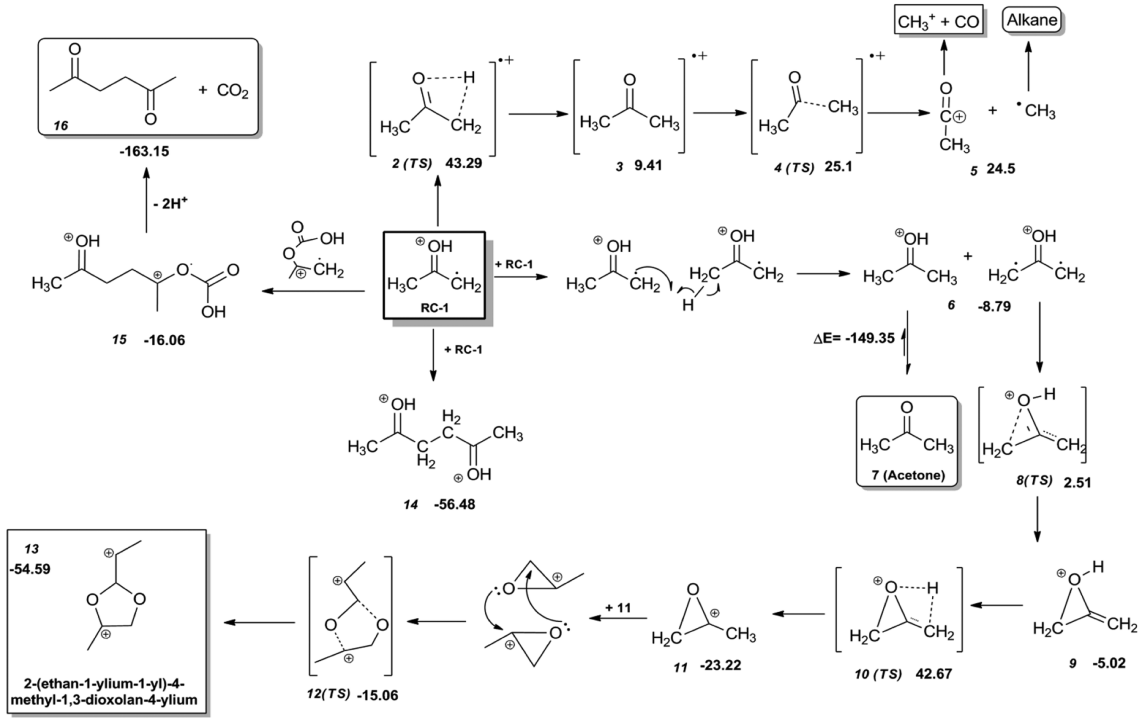

[a]Values are given in kcal mol^{-1}.

Scheme 5. Termination Path for Acetone Radical Calculated with SMD-B3LYP/6-311++G(d,p)[a]

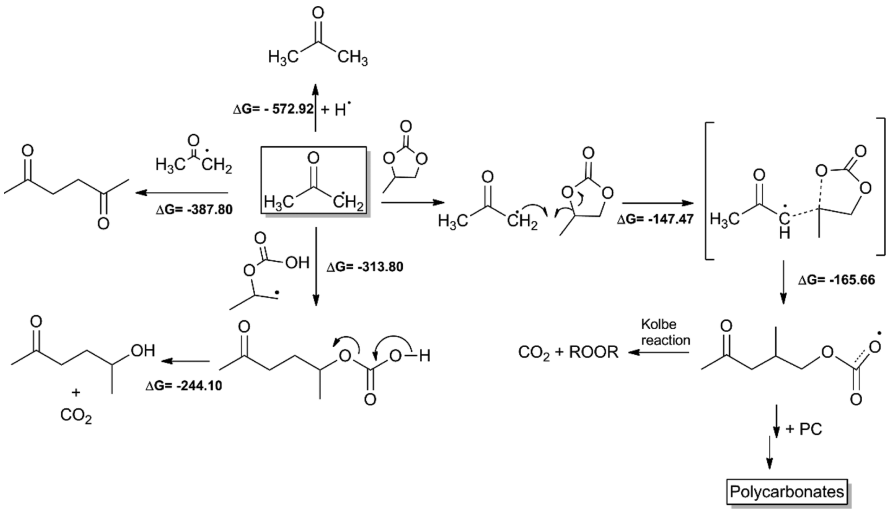

[a]Values are given in kcal mol^{-1}.

H-shift will occur through energetically demanding transition state, **2(TS)**, to give the keto isomer, which then dissociates nonergodically, favoring the departure of the newly formed methyl group as a radical and acetyl cation (**5**).[53] The

dx.doi.org/10.1021/jp403436u | J. Phys. Chem. A 2013, 117, 7959−7969

preferential cleavage of the newly formed methyl group has been confirmed by photoionization mass spectrometry experiments[54] and ab initio direct classical trajectory investigations.[55] It should be noted that alkanes are experimentally reported as one of the products formed as a result of oxidative decomposition of PC-based electrolytes.[20]

A barrierless homocoupling or dimerization reaction of **RC-1** could occur to form a dioxonium species (**14**), which is the enol form of hexane-2,5-dione (**16**). Another possible reaction of **RC-1** is a coupling reaction with the carbocation radical formed as an intermediate in the oxidative decomposition reactions, which are discussed above. This radical coupling reaction generates a monoester of carbonic acid, which is unstable and can easily undergo decarboxylation reaction to yield hexane-2,5-dione (**16**) and carbon dioxide. There is also the possibility of abstraction of the methyl hydrogen of one molecule of **RC-1** by the radical center of another. This reaction, which is a typical example of hydrogen abstractions by free radicals, proceeds to give enol form of the keto isomer of acetone (**7**) and a new diradical cation that can undergo cyclization reaction to give methyoxirane (**11**). Ring-opening via bond cleavage of the sterically hindered C−O of the two methyloxirane occurs, in accordance with the cationic ring-opening mechanism, which proceeds to form a new C−O bond and subsequently generate 2-ethyl-4-methyl-1,3-dioxolane cation (**13**).

Similarly, the termination reactions of the acetone radical, which is formed as one of the primary products in the PC-ClO_4^- oxidation, are investigated comprehensively, as presented in Scheme 5. Moreover, we have shown that in the oxidative decomposition reactions of PC-PF_6^-, PC-BF_4^-, and PC-AsF_6^- there is also a possibility of formation of acetone radical following the path that proceeds without conformational change along the H−O−C-O dihedral angle. As can be seen from Scheme 5, the acetone radical can undergo dimerization reaction to give hexane-2,5-dione, which has a significantly higher ΔG value compared with the nucleophilic attack on the ethereal C−O bond of the solvent molecule, which leads to the formation of polycarbonates (−387.80 vs −165.66 kcal mol^{-1}). It can be assumed that whenever two such radicals come in proximity they will collide and react to generate a dimer. Nevertheless, for effective combination we need to have a high concentration of radicals, which is difficult to achieve because the radicals involved in the reaction have a short lifetime as a result of reaction with other molecules. However, the ΔG values for the dimerization and radical coupling reactions are considerably negative, showing the possibility for the formation of the corresponding termination products. This observation might be associated with the phenomena called "cage effect",[56,57] in which radicals generated in solution are held in proximity and will have a high probability of undergoing dimerization reaction. Even though the concentration of the radicals is low, a solvent shell or "cage" surrounds the two radical increasing the collusion between the two before breaking through the "cage".[58]

To compare the stabilities of the final oxidative decomposition products in the electrolyte, we calculated the relative Gibbs free-energy changes (in kcal mol^{-1}) of the species identified in the termination path of **RC-1**, and values are tabulated in Table 7. From the free-energy change data, we can conclude that regardless of the type of salt used the final oxidative decomposition products, such as 2-(ethan-1-ylium-1-yl)-4-methyl-1,3-dioxolan-4-ylium (**13**), acetone (**7**), and hexane-2,5-dione (**16**), are similar. On the basis of the above discussion, the primary and final oxidative decomposition products of solvent−anion complexes mainly consist of CO_2, acetone, diketone compounds, and some polymerizable species. It should be noted that other than the diketone species all of the species identified in this study have been observed experimentally as a surface film formed on the cathode surface under abused conditions.

Table 7. Relative Gibbs Free-Energy Changes (in kcal mol^{-1}) of the Species Identified in the Termination Path of RC-1 Calculated with SMD-B3LYP/6-311++G(d,p)

structure	PC-PF_6^-	PC-AsF_6^-	PC-BF_4^-
2 (TS)	−17.57	−11.92	−26.98
3	−52.08	−46.45	−61.50
4 (TS)	−37.65	−32.20	−47.06
5	−38.90	−33.29	−48.32
6	−102.91	−91.62	−121.74
7 (acetone)	−210.22	−204.57	−219.63
8 (TS)	−111.70	−100.40	−130.05
9	−119.23	−107.93	−138.05
10 (TS)	−71.54	−60.24	−90.36
11	−138.05	−126.76	−156.88
12 (TS)	−116.22	−105.42	−135.54
13	−156.25	−144.96	−175.06
14	−163.15	−154.37	−184.49
15	−99.74	−96.00	−111.06
16 (hexane-2,5-dione)	−252.26	−246.61	−261.67

Comparison with Oxidation Mechanism of EC−Anion Complexes. Even though their reaction products have not yet been understood due to the structural similarity between EC and PC, the electrochemical oxidation mechanism of EC may be similar to that of PC. The potential-energy profiles for the oxidative decomposition of EC−anion complexes in solution are presented in Figures S2−S5 in the Supporting Information. Similar to what has been observed for the PC−anion systems, the bond between the ethereal oxygen and alkyl carbon is the weakest in all EC−anion complexes, which results in the breaking of the bond to form an open-chain cation radical. This is also in agreement with the electron-spin-resonance study by Matsuta et al.[59] and the recent work by Xing and Borodin[60] on the oxidation-induced reactions of EC.

The energy barrier for the heterolytic ring-opening reaction of [EC-PF_6^-]-e, which proceeds to give the open-chain radical, is relatively higher than that of [PC-PF_6^-]-e (14.10 vs 12.51 kcal mol^{-1}, respectively). Decarboxylation reaction of this radical, which generates acetaldehyde radical, HF, CO_2, and PF_5, is more favorable than the corresponding step in [PC-PF_6^-], as seen from the energy barrier, which is 3.02 kcal mol^{-1} less than that of TS1-4. However, the energy barrier for the rate-determining step, which gives vinyl alcohol radical, CO_2, and PF_6^-, is higher than the corresponding path in the oxidative decomposition reaction of PC-PF_6^-. By using in situ FTIR measurements, Matsushita et al.[61] observed the formation of species having carboxylic groups on the cathode material due to the oxidation of EC. It can be speculated that the carboxylic acid species detected may arise as a result of the oxidation of the acetaldehyde species, which is, as discussed above, identified as one of the primary oxidation products. Moreover, the formation of vinyl alcohol radical will probably lead to the generation of polymerized species at the electrode surface, as reported in the previous studies.[60,62]

Even though, from a mechanistic point of view, the oxidative decomposition mechanism of EC-AsF_6^- and EC-BF_4^- follows a similar path as EC-PF_6^-, the energy barrier for the heterolytic ring-opening steps in the decomposition paths of EC-BF_4^- is lower than that of EC-AsF_6^- by ∼8.69 kcal mol^{-1}. The corresponding reactions in the oxidative decomposition of PC−anion complexes show lower energy barriers due to the difference in reactivity between PF_6^-, BF_4^-, and AsF_6^- with PC and EC. As can be seen from Figure S5 in the Supporting Information and Figure 5, the oxidative decomposition mechanism of EC-ClO_4^- is similar to the analogous path in PC-ClO_4^- because both proceed through ring-opening reaction via the cleavage of the bond between the alkyl carbon and ethereal oxygen. The heterolytic ring-opening reaction in EC-ClO_4^- oxidation happens with ring-opening barrier of 7.53 kcal mol^{-1}, which is 3.14 kcal mol^{-1} higher than the parallel reaction in PC-ClO_4^- and generates CO_2, $HClO_4$, and acetaldehyde radical as primary oxidation products. The values of energy barriers for the rate-determining states in the oxidative decomposition of EC−anion complex suggest that CO_2 would generate from the intermediates, even at room temperature. However, compared with the analogous reactions in PC−anion complex, the CO_2 generation in the former will likely be smaller than the latter. A similar conclusion was also made by Joho and Novák,[62] who compared the oxidative decomposition of carbonate-based electrolytes by using in situ FTIR techniques.

Because EC has higher oxidation potential than PC, PC will more readily oxidize to form a protective film on the cathode. However, despite the fact that PC-based solutions are attractive as electrolyte solutions for lithium ion batteries, it is well known that PC has poor compatibility with graphite anode due to excessive solvent decomposition.[63] One approach to harness the advantages of PC without compromising the graphite anode is to use PC in low concentration as a cosolvent together with EC or other nonaqueous solvents. Because the rate of production of gas was observed to be dependent on the type of salt used, the oxidative decomposition reactions of PC can be controlled by designing appropriate lithium salts. It should be noted that previously reported experimental works showed that certain salts can stabilize graphitic anode materials in neat PC without the risk of exfoliation.[64,65]

CONCLUSIONS

DFT calculations have been carried out to understand the oxidative decomposition mechanism of propylene carbonate in the presence of lithium salts ($LiClO_4$, $LiBF_4$, $LiPF_6$, and $LiAsF_6$). Energetic calculations suggest that the initial oxidative decomposition products of PC-PF_6^-, PC-AsF_6^-, and PC-BF_4^- are CO_2, the enol form of acetone cation radical, and acetone radical. However, PC-ClO_4^-directly generates CO_2, $HClO_4$, and acetone radical as primary oxidation products which is attributed to the highly resonance stabilized structure of the perchlorate anion. The oxidative decomposition reactions of the fluorinated acid base adducts are catalyzed by the anion and the acid, which is formed in the initial step. Termination of the primary radicals formed as a primary oxidation product will produce polycarbonate, acetone, diketone, 2-(ethan-1-ylium-1-yl)-4-methyl-1,3-dioxolan-4-ylium, and CO_2. Although, EC−anion complexes initially follow the same decomposition mechanism as PC, it was found that the primary oxidative decomposition products of EC differ substantially from those of PC−anion complexes.

Even though the major oxidation products of PC are independent of the kind of electrolyte salt used, the CO_2 generation, as well as the stability of the oxidation products formed are highly influenced by the type of salt employed. On the basis of the thermodynamic and kinetic data, PC-oxidation resulting in gas generation is enhanced in the $[PC\text{-}ClO_4]^-$. The rate constant calculated using TST confirms the gas volume generation is to be on the order of $[PC\text{-}ClO_4]^- > [PC\text{-}BF_4]^- > [PC\text{-}AsF_6]^- > [PC\text{-}PF_6]^-$.

ASSOCIATED CONTENT

Supporting Information

Optimized geometries for neutral and oxidized species, bond orders for oxidized PC−anion complexes, and vibrational, electronic, translational, rotational, calculated molecular partition functions, and potential energy profiles for the oxidative decomposition of EC−anion complexes are given. This material is available free of charge via the Internet at http://pubs.acs.org.

AUTHOR INFORMATION

Corresponding Author

*E-mail: jcjiang@mail.ntust.edu.tw.

Notes

The authors declare no competing financial interest.

ACKNOWLEDGMENTS

This work was supported by the Ministry of Economic Affairs of Taiwan, ROC (101-EC-17-A-08-S1-183). We are also grateful to the National Center of High-Performance Computing for computer time and facilities.

REFERENCES

(1) Jansen, A. N.; Kahaian, A. J.; Kepler, K. D.; Nelson, P. A.; Amine, K.; Dees, D. W.; Vissers, D. R.; Thackeray, M. M. Development of a High-Power Lithium-Ion Battery. *J. Power Sources* **1999**, *81*−*82*, 902−905.

(2) Scrosati, B. Recent Advances in Lithium Ion Battery Materials. *Electrochim. Acta* **2000**, *45*, 2461−2466.

(3) Scrosati, B. History of Lithium Batteries. *J. Solid State Electrochem.* **2011**, 1−8.

(4) Megahed, S.; Ebner, W. Lithium-Ion Battery for Electronic Applications. *J. Power Sources* **1995**, *54*, 155−162.

(5) Tarascon, J. M.; Armand, M. Issues and Challenges Facing Rechargeable Lithium Batteries. *Nature* **2001**, *414*, 359−367.

(6) Sun, Y.-K.; Myung, S.-T.; Park, B.-C.; Prakash, J.; Belharouak, I.; Amine, K. High-Energy Cathode Material for Long-Life and Safe Lithium Batteries. *Nat. Mater.* **2009**, *8*, 320−324.

(7) Sun, Y.-K.; Lee, B.-R.; Noh, H.-J.; Wu, H.; Myung, S.-T.; Amine, K. A Novel Concentration-Gradient $Li[Ni_{0.83}Co_{0.07}Mn_{0.10}]O_2$ Cathode Material for High-Energy Lithium-Ion Batteries. *J. Mater. Chem.* **2011**, *21*, 10108−10112.

(8) Cho, Y.; Lee, S.; Lee, Y.; Hong, T.; Cho, J. Spinel-Layered Core-Shell Cathode Materials for Li-Ion Batteries. *Adv. Energy Mater.* **2011**, *1*, 821−828.

(9) Novak, P.; Christensen, P. A.; Iwasita, T.; Vielstich, W. Anodic Oxidation of Propylene Carbonate on Platinum, Glassy Carbon and Polypyrrole: An "In-Situ" FTIR Study. *J. Electroanal. Chem. Interfacial Electrochem.* **1989**, *263*, 37−48.

(10) Wang, Q.; Ping, P.; Zhao, X.; Chu, G.; Sun, J.; Chen, C. Thermal Runaway Caused Fire and Explosion of Lithium Ion Battery. *J. Power Sources* **2012**, *208*, 210−224.

(11) Vetter, J.; Novák, P.; Wagner, M. R.; Veit, C.; Möller, K. C.; Besenhard, J. O.; Winter, M.; Wohlfahrt-Mehrens, M.; Vogler, C.; Hammouche, A. Ageing Mechanisms in Lithium-Ion Batteries. *J. Power Sources* **2005**, *147*, 269−281.

(12) Balakrishnan, P. G.; Ramesh, R.; Prem Kumar, T. Safety Mechanisms in Lithium-Ion Batteries. *J. Power Sources* **2006**, *155*, 401−414.
(13) Nishi, Y. Lithium Ion Secondary Batteries; Past 10 Years and the Future. *J. Power Sources* **2001**, *100*, 101−106.
(14) Xu, K. Nonaqueous Liquid Electrolytes for Lithium-Based Rechargeable Batteries. *Chem. Rev.* **2004**, *104*, 4303−4418.
(15) Zhang, X.; Pugh, J. K.; Ross, P. N. Computation of Thermodynamic Oxidation Potentials of Organic Solvents Using Density Functional Theory. *J. Electrochem. Soc.* **2001**, *148*, E183−E188.
(16) Yamaki, J.-i. Liquid Electrolytes. In *Advances In Lithium-Ion Batteries*; Schalkwijk, W., Scrosati, B., Eds.; Kluwer Academic: New York, 2002; pp 155−183.
(17) Aurbach, D.; Levi, M. D.; Levi, E.; Teller, H.; Markovsky, B.; Salitra, G.; Heider, U.; Heider, L. Common Electroanalytical Behavior of Li Intercalation Processes into Graphite and Transition Metal Oxides. *J. Electrochem. Soc.* **1998**, *145*, 3024−3034.
(18) Kanamura, K.; Umegaki, T.; Ohashi, M.; Toriyama, S.; Shiraishi, S.; Takehara, Z.-i. Oxidation of Propylene Carbonate Containing $LiBF_4$ or $LiPF_6$ on $LiCoO_2$ Thin Film Electrode for Lithium Batteries. *Electrochim. Acta* **2001**, *47*, 433−439.
(19) Kanamura, K.; Toriyama, S.; Shiraishi, S.; Takehara, Z. i. Studies on Electrochemical Oxidation of Nonaqueous Electrolytes Using In Situ FTIR Spectroscopy: I. The Effect of Type of Electrode on On-Set Potential for Electrochemical Oxidation of Propylene Carbonate Containing 1.0 mol dm^{-3}. *Electrochim. Acta* **1995**, *142*, 1383−1389.
(20) Arakawa, M.; Yamaki, J.-i. Anodic Oxidation of Propylene Carbonate and Ethylene Carbonate on Graphite Electrodes. *J. Power Sources* **1995**, *54*, 250−254.
(21) Xing, L.; Wang, C.; Li, W.; Xu, M.; Meng, X.; Zhao, S. Theoretical Insight into Oxidative Decomposition of Propylene Carbonate in the Lithium Ion Battery. *J. Phys. Chem. B* **2009**, *113*, 5181−5187.
(22) Xing, L.; Borodin, O.; Smith, G. D.; Li, W. Density Functional Theory Study of the Role of Anions on the Oxidative Decomposition Reaction of Propylene Carbonate. *J. Phys. Chem. A* **2011**, *115*, 13896−13905.
(23) Xing, L.; Li, W.; Wang, C.; Gu, F.; Xu, M.; Tan, C.; Yi, J. Theoretical Investigations on Oxidative Stability of Solvents and Oxidative Decomposition Mechanism of Ethylene Carbonate for Lithium Ion Battery Use. *J. Phys. Chem. B* **2009**, *113*, 16596−16602.
(24) Li, M.; Liu, W.; Peng, C.; Ren, Q.; Lu, W.; Deng, W. A DFT Study on Reaction of Eupatilin with Hydroxyl Radical in Solution. *Int. J. Quantum Chem.* **2013**, *113*, 966−974.
(25) Scheiner, S. Evaluation of DFT Methods to Study Reactions of Benzene with OH Radical. *Int. J. Quantum Chem.* **2012**, *112*, 1879−1886.
(26) Sangha, A. K.; Parks, J. M.; Standaert, R. F.; Ziebell, A.; Davis, M.; Smith, J. C. Radical Coupling Reactions in Lignin Synthesis: A Density Functional Theory Study. *J. Phys. Chem. B* **2012**, *116*, 4760−4768.
(27) Izgorodina, E. I.; Brittain, D. R. B.; Hodgson, J. L.; Krenske, E. H.; Lin, C. Y.; Namazian, M.; Coote, M. L. Should Contemporary Density Functional Theory Methods be Used to Study the Thermodynamics of Radical Reactions? *J. Phys. Chem. A* **2007**, *111*, 10754−10768.
(28) Zhao, Y.; Truhlar, D. G. How Well Can New-Generation Density Functionals Describe the Energetics of Bond-Dissociation Reactions Producing Radicals? *J. Phys. Chem. A* **2008**, *112*, 1095−1099.
(29) Nguyen, M. T.; Creve, S.; Vanquickenborne, L. G. Difficulties of Density Functional Theory in Investigating Addition Reactions of the Hydrogen Atom. *J. Phys. Chem.* **1996**, *100*, 18422−18425.
(30) Nguyen, H. M. T.; Peeters, J.; Nguyen, M. T.; Chandra, A. K. Use of DFT-Based Reactivity Descriptors for Rationalizing Radical Reactions: A Critical Analysis. *J. Phys. Chem. A* **2003**, *108*, 484−489.
(31) Wu, Q.; Liang, G.; Zu, L.; Fang, W. Vibrationally Resolved LIF Spectrum of Tertiary Methylcyclohexoxy Radical. *J. Phys. Chem. A* **2012**, *116*, 3156−3162.
(32) Lee, C.; Yang, W.; Parr, R. G. Development of the Colle-Salvetti Correlation-Energy Formula into a Functional of the Electron Density. *Phys. Rev. B* **1988**, *37*, 785−789.
(33) Becke, A. D. Density-Functional Thermochemistry. III. The Role of Exact Exchange. *J. Chem. Phys.* **1993**, *98*, 5648.
(34) Stephens, P. J.; Devlin, F. J.; Chabalowski, C. F.; Frisch, M. J. Ab Initio Calculation of Vibrational Absorption and Circular Dichroism Spectra Using Density Functional Force Fields. *J. Phys. Chem.* **1994**, *98*, 11623−11627.
(35) Vosko, S. H.; Wilk, L.; Nusair., M. Accurate Spin-Dependent Electron Liquid Correlation Energies for Local Spin Density Calculations: A Critical Analysis. *Can. J. Phys* **1980**, *58*, 1200−1211.
(36) Frisch, M. J.; Trucks, G. W.; Schlegel, H. B.; Scuseria, G. E.; Robb, M. A.; Cheeseman, J. R.; Montgomery, J. A., Jr.; Vreven, T.; Kudin, K. N.; Burant, J. C.; et al. *Gaussian 09*, revision A.1; Gaussian, Inc.: Wallingford, CT, 2009.
(37) Jensen, F. *Introduction to Computational Chemistry*, 2nd ed.; John Wiley & Sons, Ltd: Chichester, U.K., 2007.
(38) Glendening, E. D.; Reed, A. E.; Carpenter, J. E.; Weinhold, F. *NBO*, version 3.1.
(39) Marenich, A. V.; Cramer, C. J.; Truhlar, D. G. Universal Solvation Model Based on Solute Electron Density and on a Continuum Model of the Solvent Defined by the Bulk Dielectric Constant and Atomic Surface Tensions. *J. Phys. Chem. B* **2009**, *113*, 6378−6396.
(40) Fang, J.; Kelarakis, A.; Lin, Y.-W.; Kang, C.-Y.; Yang, M.-H.; Cheng, C.-L.; Wang, Y.; Giannelis, E. P.; Tsai, L.-D. Nanoparticle-Coated Separators for Lithium-Ion Batteries with Advanced Electrochemical Performance. *Phys. Chem. Chem. Phys.* **2011**, *13*, 14457−14461.
(41) DiLeo, R. A.; Castiglia, A.; Ganter, M. J.; Rogers, R. E.; Cress, C. D.; Raffaelle, R. P.; Landi, B. J. Enhanced Capacity and Rate Capability of Carbon Nanotube Based Anodes with Titanium Contacts for Lithium Ion Batteries. *ACS Nano* **2010**, *4*, 6121−6131.
(42) McQuarrie, D. A.; Simon, J. D. *Physical Chemistry: A Molecular Approach*; University Science Books: Sausalito, CA, 1997.
(43) Roy, L. E.; Jakubikova, E.; Guthrie, M. G.; Batista, E. R. Calculation of One-Electron Redox Potentials Revisited. Is It Possible to Calculate Accurate Potentials with Density Functional Methods? *J. Phys. Chem. A* **2009**, *113*, 6745−6750.
(44) Linstrom, P. J.; Mallard, W. G. *NIST Chemistry WebBook*; NIST Standard Reference Database Number 69; National Institute of Standards and Technology: Gaithersburg, MD. http://webbook.nist.gov (retrieved July 19, 2012).
(45) Aurbach, D.; Gamolsky, K.; Markovsky, B.; Gofer, Y.; Schmidt, M.; Heider, U. On the Use of Vinylene Carbonate (VC) as an Additive to Electrolyte Solutions for Li-ion Batteries. *Electrochim. Acta* **2002**, *47*, 1423−1439.
(46) Tobishima, S.-I.; Yamaji, A. Ethylene Carbonate—Propylene Carbonate Mixed Electrolytes for Lithium Batteries. *Electrochim. Acta* **1984**, *29*, 267−271.
(47) Cattaneo, E.; Rasch, B.; Vielstich, W. Anodic Stability of Propylene Carbonate Electrolytes at Potentials above 4 V Against Lithium: An On-line MS and in Situ FTIR Study. *J. Appl. Electrochem.* **1991**, *21*, 885−894.
(48) Borodin, O. Polarizable Force Field Development and Molecular Dynamics Simulations of Ionic Liquids. *J. Phys. Chem. B* **2009**, *113*, 11463−11478.
(49) Vatamanu, J.; Borodin, O.; Bedrov, D.; Smith, G. D. Molecular Dynamics Simulation Study of the Interfacial Structure and Differential Capacitance of Alkylimidazolium Bis(trifluoromethanesulfonyl)-imide [$C_n$mim][TFSI] Ionic Liquids at Graphite Electrodes. *J. Phys. Chem. C* **2012**, *116*, 7940−7951.
(50) Xue, Z.-M.; Chen, C.-H. Density Functional Theory Study on Lithium Bis[1,2-benzenediolato(2-)-O,O′] borate and its Derivatives:

Electronic Structures, Energies, and Molecular Properties. *Electrochim. Acta* **2004**, *49*, 5167−5175.
(51) Xue, Z.; Ding, Y.; Chen, C. A DFT Study of Electronic Structures, Energies, and Molecular Properties of Lithium bis-[croconato]borate and its Derivatives. *Electrochim. Acta* **2007**, *53*, 990−997.
(52) Woodward, R. B.; Hoffmann, R. The Conservation of Orbital Symmetry. *Angew. Chem., Int. Ed.* **1969**, *8*, 781−853.
(53) Hudson, C. E.; McAdoo, D. J. Circumvention of Orbital Symmetry Restraints by 1,3-H-shifts of Enolic Radical Cations. *J. Am. Soc. Mass Spectrom.* **2004**, *15*, 972−981.
(54) McAdoo, D. J. Contributions of $C_3H_6O^{+\cdot}$ ions with the Oxygen on the Middle Carbon to Gas Phase Ion Chemistry. *Mass Spectrom. Rev.* **2000**, *19*, 38−61.
(55) Zhou, J.; Schlegel, H. B. Dissociation of Acetone Radical Cation ($CH_3COCH_3^{+\cdot} \rightarrow CH_3CO^+ + CH_3\cdot$): An Ab Initio Direct Classical Trajectory Study of the Energy Dependence of the Branching Ratio. *J. Phys. Chem. A* **2008**, *112*, 13121−13127.
(56) Niki, E.; Kamiya, Y. Cage Reactions of tert-Butoxy Radicals. Effects of Solvent and Viscosity. *J. Am. Chem. Soc.* **1974**, *96*, 2129−2133.
(57) Lorand, J. P. The Cage Effect. In *Progress in Inorganic Chemistry*; John Wiley & Sons, Inc.: New York, 2007; pp 207−325.
(58) Leggesse, E. G.; Jiang, J.-C. Theoretical Study of the Reductive Decomposition of 1,3-Propane Sultone: SEI Forming Additive in Lithium-Ion Batteries. *RSC Adv.* **2012**, *2*, 5439−5446.
(59) Matsuta, S.; Kato, Y.; Ota, T.; Kurokawa, H.; Yoshimura, S.; Fujitani, S. Electron-Spin-Resonance Study of the Reaction of Electrolytic Solutions on the Positive Electrode for Lithium-Ion Secondary Batteries. *J. Electrochem. Soc.* **2001**, *148*, A7−A10.
(60) Xing, L. D.; Borodin, O. Oxidation Induced Decomposition of Ethylene Carbonate from DFT Calculations - Importance of Explicitly Treating Surrounding Solvent. *Phys. Chem. Chem. Phys.* **2012**, *14*, 12838−12843.
(61) Matsushita, T.; Dokko, K.; Kanamura, K. In situ FT-IR Measurement for Electrochemical Oxidation of Electrolyte with Ethylene Carbonate and Diethyl Carbonate on Cathode Active Material used in Rechargeable Lithium Batteries. *J. Power Sources* **2005**, *146*, 360−364.
(62) Joho, F.; Novák, P. SNIFTIRS Investigation of the Oxidative Decomposition of Organic-Carbonate-Based Electrolytes for Lithium-Ion Cells. *Electrochim. Acta* **2000**, *45*, 3589−3599.
(63) Chung, G. C.; Kim, H. J.; Yu, S. I.; Jun, S. H.; Choi, J. w.; Kim, M. H. Origin of Graphite Exfoliation An Investigation of the Important Role of Solvent Cointercalation. *J. Electrochem. Soc.* **2000**, *147*, 4391−4398.
(64) Xu, K.; Zhang, S.; Poese, B. A.; Jow, T. R. Lithium Bis(oxalato)borate Stabilizes Graphite Anode in Propylene Carbonate. *Electrochem. Solid-State Lett.* **2002**, *5*, A259−A262.
(65) Jeong, S.-K.; Inaba, M.; Iriyama, Y.; Abe, T.; Ogumi, Z. Electrochemical Intercalation of Lithium Ion within Graphite from Propylene Carbonate Solutions. *Electrochem. Solid-State Lett.* **2003**, *6*, A13−A15.